Original Research Article

# Structure-Based Comparative Docking Analysis of Fungal Metabolites Against NDM-Family Metallo-β-Lactamases

Jayden Cho

*The Early College at Guilford, 5608 W Friendly Ave, Greensboro, North Carolina, 27410, United States*

## ABSTRACT

Carbapenemase-producing bacteria are a major global health concern because they can hydrolyze a broad range of β-lactam antibiotics, including carbapenems that are often used as last-resort treatments. Among these enzymes, New Delhi metallo-β-lactamases (NDMs) are particularly problematic due to their broad substrate spectrum, rapid global dissemination, and the limited availability of clinically effective inhibitors. In this study, a structure-based docking analysis of selected fungal metabolites against NDM-family metallo-β-lactamases was performed. Seventeen fungal metabolites were initially screened, and eight compounds were selected for docking against eight experimentally resolved NDM-family structures using CB-Dock2. The resulting complexes were further examined and visualized using UCSF Chimera. Protein-ligand interactions were analyzed using PLIP and electrostatic surface mapping. An empirical cutoff (Vina score ≤ −8.0 kcal/mol) was used as a practical prioritization criterion rather than as a predictor of inhibitory activity. Pulvinic acid, Pseurotin A, Hispidin, and Scytalone were prioritized for further analysis. Hispidin and Scytalone tended to localize near catalytic regions, whereas Pulvinic acid and Pseurotin A more frequently occupied adjacent or substrate-entry regions. Reference β-lactamase inhibitors were included to provide structural context for docking interpretation. These ligands localized within predicted binding regions and provided a basis for comparison with fungal metabolites. None of the compounds demonstrated direct $Zn^{2+}$ coordination, suggesting that classical zinc-chelation-based inhibition is unlikely. ADMET predictions indicated that Hispidin and Scytalone possess relatively favorable drug-like properties, whereas Pulvinic acid and Pseurotin A may serve as initial scaffolds for further optimization. Overall, this study highlights fungal natural products as structurally diverse compounds that may serve as useful starting points for exploring ligand interactions with NDM-family metallo-β-lactamases and generating hypotheses for future inhibitor development.

**Keywords:** carbapenemases; metallo-β-lactamases; protein-ligand interactions (PLIP); *in silico* docking; fungal metabolites; antibiotic resistance

**Corresponding author:** Jayden Cho, E-mail: jcho6069@gmail.com.

**Accepted** June 15, 2026
https://doi.org/10.70251/HYJR2348.43568591

## INTRODUCTION

β-lactam antibiotics are a group of drugs that can kill bacteria by disrupting their protective cell walls. These antibiotics are named after a characteristic β-lactam ring in their chemical structure. Bacteria rely on strong cell

walls for survival; however, β-lactam antibiotics inhibit the enzymes involved in cell wall synthesis (penicillin-binding proteins), leading to weakened cell walls and bacterial death (1). Common β-lactam antibiotics include penicillins, cephalosporins, carbapenems, and monobactams (2). Over time, bacteria have evolved mechanisms to resist these antibiotics, most notably through the production of β-lactamases, which hydrolyze the β-lactam ring and render the drugs ineffective (3). As new antibiotics have been developed, β-lactamases have continued to evolve, resulting in variants capable of inactivating even last-resort antibiotics such as carbapenems (4). Therefore, there is a continued need to investigate β-lactamase interactions, develop new antibiotics, and explore natural compounds that may interact with these enzymes.

Carbapenem-resistant Enterobacterales (CRE) represent one of the most critical threats to global public health. According to the Centers for Disease Control and Prevention, New Delhi metallo-β-lactamase-producing CRE (NDM-CRE) increased by approximately 460% between 2019 and 2023 in the U.S. (5). These pathogens can cause severe infections, including pneumonia, bloodstream infections, and wound infections, and are difficult to treat due to limited effective antibiotics (6). Their resistance is primarily driven by carbapenemases, a diverse group of β-lactamases capable of hydrolyzing carbapenems (7). Carbapenemases include both serine-based enzymes (e.g., KPC [class A], OXA-48 [class D]) and metallo-β-lactamases (MBLs; e.g., NDM, VIM, IMP [class B]), which differ in catalytic mechanisms and structural features (8). Among MBLs, NDM enzymes are of particular concern due to their widespread dissemination and ability to hydrolyze a broad range of β-lactam antibiotics (9, 10). Consequently, NDM enzymes were selected as the primary targets of this study. While inhibitors targeting these enzymes are of interest for restoring antibiotic efficacy, their development remains challenging (13). In particular, effective inhibition of MBLs often involves direct interaction with $Zn^{2+}$ ions in the catalytic site (11, 12).

Fungi are organisms that must compete with bacteria and other microbes to survive in natural environments. To support their survival, fungi produce a wide range of secondary metabolites with diverse chemical structures. Many of these compounds exhibit antibacterial activity, reflecting a long-standing ecological "chemical arms race." Their metabolites encompass structurally diverse classes such as polyketides, nonribosomal peptides, alkaloids, and terpenoids, often featuring unique scaffolds not represented in conventional synthetic libraries (14). Historically, fungal-derived natural products have played a central role in antibiotic discovery, including penicillin, cephalosporins, and fusidic acid (15). However, relatively few studies have examined fungal metabolites in the context of carbapenemase interaction.

Recent progress in computational screening has enabled rapid assessment of natural products using molecular docking and structural interaction analyses, offering an efficient strategy to prioritize candidates for further investigation (16). In this work, a structure-based *in silico* approach was applied to explore how selected fungal metabolites interact with NDM-family metallo-β-lactamases. Docking simulations were combined with protein-ligand interaction profiling and solvent-accessible surface analysis to examine binding orientation and key interaction features across multiple experimentally resolved NDM structures. In parallel, *in silico* ADMET predictions were conducted to evaluate general drug-likeness and support compound selection. It should be noted that docking scores and static binding conformations were not considered indicators of inhibitory activity; instead, they were used to enable comparative structural interpretation and guide hypothesis development. The overall aim was to identify fungal-derived scaffolds capable of interacting with NDM-family metallo-β-lactamases and to provide a structural basis for subsequent experimental validation rather than to claim functional inhibition.

## METHODS AND MATERIALS

### Target Protein/Receptor Preparation

Receptor candidates related to NDM enzymes were identified in the RCSB Protein Data Bank (PDB) using the keyword "NDM" to obtain structurally relevant protein models for molecular docking (Table 1) (17). Eight NDM-family metallo-β-lactamase structures (PDB IDs: 3S0Z, 4EXS, 4TZ9, 5YPI, 5YPN, 6OVZ, 6XBF, and 7VQJ) were downloaded from the Protein Data Bank in PDB format (Supplementary Figure 1). Water molecules and other nonessential atoms were removed from each structure, while the catalytic $Zn^{2+}$ ions were retained to preserve the active-site configuration using UCSF Chimera (v1.19) (18). The processed receptors were uploaded to CB-Dock2 (19), which automatically prepared the proteins by adding hydrogen atoms and partial charges prior to docking. The structural integrity of the Zn-binding residues was verified using UCSF Chimera (Figure 1).

***Table 1.*** *NDM-family metallo-β-lactamase receptor structures used for docking analysis.*

| PDB ID | Receptor Description | Class | Type |
|---|---|---|---|
| 3S0Z | NDM-1 | B | MBL |
| 4EXS | NDM-1-captopril complex | B | MBL |
| 4TZ9 | NDM-3 | B | MBL |
| 5YPI | NDM-1-hydrolyzed imipenem complex | B | MBL |
| 5YPN | NDM-1-hydrolyzed meropenem complex | B | MBL |
| 6OVZ | NDM-1 affinity-label adduct | B | MBL |
| 6XBF | NDM-family metallo-β-lactamase complex | B | MBL |
| 7VQJ | NDM-1-hydrolyzed ligand complex | B | MBL |

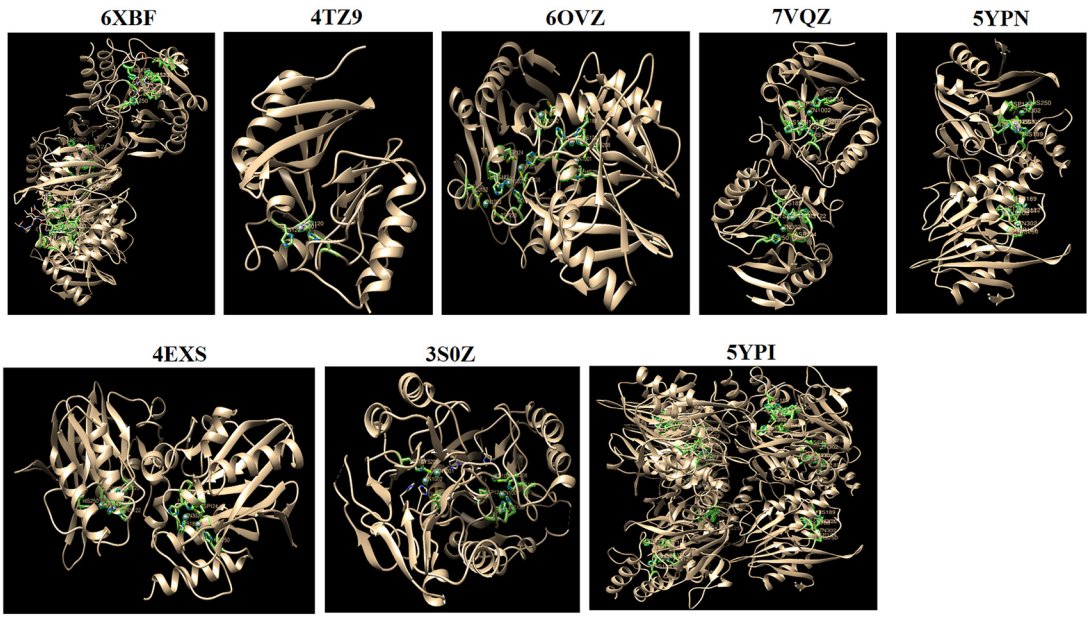


***Figure 1.*** *Three-dimensional structures of NDM-family metallo-β-lactamase receptors used for molecular docking analysis. Each structure was visualized in UCSF Chimera, highlighting the catalytic metal ions or active-site residues (shown in green).*

**Selection and Preparation of Fungal-Derived Ligands**

Seventeen fungal-derived natural products were initially identified from the ChEBI and LOTUS databases. Eight compounds (Scytalone, Aspyrone, Radicinin, Altenusin, Pseurotin A, Pulvinic acid, Hispidin, and Tricholignan A) were selected for docking analysis. These compounds were prioritized because they were listed as having no primary hazard classifications in the source databases and had complete 3D structural information available for docking. Compounds associated with hazard classifications or lacking suitable 3D structural data (e.g., Epichlicin) were excluded from further analysis. The selected compounds are indicated by an asterisk in Supplemental Table 1. The three-dimensional (3D) structures and associated chemical information for each compound were downloaded from the PubChem database (22) as 3D conformers (.sdf). To provide structural context for docking analysis, two reference β-lactamase inhibitors, avibactam (CID: 9835049) and captopril (CID: 44093), were also included as reference ligands. Their 3D structures were obtained from the PubChem database in the same format and prepared using the same workflow as the fungal-derived compounds.

**Molecular Docking Analysis (CB-Dock2)**

The 3D structures of these compounds were retrieved directly from the PubChem database in their standard formats and uploaded to the CB-Dock2 web server (23) without additional preprocessing. The docking simulations were performed in July 2025. Molecular docking was carried out automatically by CB-Dock2, and the resulting binding affinity data (Vina scores) were recorded in Microsoft Excel for further analysis. Protein-ligand complex files in PDB format were also downloaded for subsequent structural analysis. An empirical cutoff of -8.0 kcal/mol was applied as a practical prioritization criterion to select ligand-receptor complexes for further analysis. This threshold was not used as a validated indicator of binding strength or inhibitory activity. Docking scores and poses were used only to suggest possible binding modes and for comparative structural analysis, rather than to demonstrate functional inhibition. In addition, factors such as protonation, metal interactions, and solvent effects were not fully considered, which may affect the accuracy of the predicted binding results. Next, the dataset was processed in R (v4.4.2) using the pheatmap package with a red-white-blue gradient to compare relative binding patterns across receptors.

**Protein-Ligand Interaction Profiling (PLIP analysis)**

The docked complexes of selected ligand-receptor pairs (based on the prioritization criterion described above) were further analyzed using the Protein-Ligand Interaction Profiler (PLIP) (24). The top-ranked docking poses generated by CB-Dock2 were uploaded to PLIP in PDB format to identify and characterize molecular interactions. PLIP automatically detected key noncovalent interactions, including hydrogen bonds, hydrophobic contacts, π-π stacking, π-cation interactions, salt bridges, and metal coordination (25). The interaction profiles were saved in XML format and visualized as both 2D schematic diagrams and 3D structural representations, providing detailed information on the amino acid residues involved in ligand binding. Docked poses were additionally examined using UCSF Chimera to support structural interpretation.

**Structural Visualization and Solvent-Accessible Surface (SAS)**

The structural visualization of protein-ligand complexes was performed using BIOVIA Discovery Studio Visualizer (v25.1) and UCSF Chimera. The three-dimensional structures obtained from PLIP analysis were used to examine binding pocket topology, ligand orientation, and noncovalent interaction geometry. Discovery Studio Visualizer was used to display the solvent-accessible surface (SAS) of the protein and the 2D interaction model between the ligand and the active site. These images helped visualize how the ligand fits into the protein and which amino acids interact with it. To provide structural context for docking interpretation, two reference β-lactamase inhibitors, captopril and avibactam, were included in the analysis. These ligands were docked using the same CB-Dock2 workflow applied to fungal metabolites. The resulting docking poses were analyzed using PLIP to identify noncovalent interactions and were further examined in UCSF Chimera for structural validation. Reference ligands were used for comparative binding-mode analysis rather than score-based benchmarking.

***In silico* Pharmacokinetic and Drug-Likeness Evaluation**

The pharmacokinetic properties and drug-likeness of the top-performing ligands were evaluated using SwissADME (26). The chemical structures of each compound, written in standard SMILES format, were retrieved from the PubChem database and submitted to the web server to predict key absorption, distribution, metabolism, excretion, and toxicity (ADMET) parameters, including Lipinski's rule of five, topological polar surface area (TPSA), logP, water solubility, and bioavailability score (27). The BOILED-Egg model was used to evaluate whether the compounds could be absorbed in the body (HIA) and if they could enter the brain (BBB). PAINS and Brenk filters were used to identify chemical structures that could cause problems in experiments. The results provided a comprehensive view of the pharmacological suitability of the ligands selected from docking and interaction analysis.

The SMILES of the compounds/ligands are listed below.

| | |
|---|---|
| Hispidin | C1=CC(=C(C=C1/C=C/C2=CC(=CC(=O)O2)O)O)O |
| Scytalone | C1[C@H](CC(=O)C2=C1C=C(C=C2O)O)O |
| Pseurotin A | CC/C=C\[C@@H]([C@@H](C1=C(C(=O)[C@@]2(O1)[C@H]([C@@](NC2=O)(C(=O)C3=CC=CC=C3)OC)O)C)O)O |
| Pulvinic acid | C1=CC=C(C=C1)C2=C(/C(=C(/C3=CC=CC=C3)\C(=O)O)/OC2=O)O |

## RESULTS AND DISCUSSION

### Primary Docking

This study intentionally avoids interpreting docking scores or poses as indicators of functional inhibition and instead focuses on comparative structural analysis across multiple NDM-family metallo-β-lactamase structures. The CB-Dock2 docking analysis identified several fungal-derived metabolites that exhibited favorable predicted binding affinities against the selected receptor panel. The docking heatmap (Figure 2) presents the Vina scores for eight ligands tested across eight NDM-family metallo-β-lactamase structures, where more negative values indicate stronger predicted binding. Across all docking simulations, Vina scores ranged from -5.1 to -9.2 kcal/mol, suggesting that several metabolites may form energetically favorable interactions within the receptor structures (Supplemental Table 2). These observations indicate that certain compounds may associate with structurally and catalytically relevant regions of NDM-family enzymes.

Pulvinic acid exhibited the highest predicted affinity, particularly toward the NDM-1 structure represented by PDB ID 6OVZ, where the Vina score reached -9.2 kcal/mol. Other notable interactions included Pseurotin A with NDM-1 (6XBF, -9.0 kcal/mol) and Hispidin with 5YPI (-8.4 kcal/mol). Cavity volumes of 200-500 Å³ generally correspond to typical drug-like binding pockets, whereas larger volumes may represent more open binding regions. Although the predicted cavity volume associated with Hispidin was relatively large, this does not necessarily indicate an unreliable docking result. CB-Dock2 may occasionally identify broader binding regions rather than highly confined pockets. Despite the large cavity volume, Hispidin was localized near the catalytic $Zn^{2+}$ ions and interacted with neighboring residues within the active-site region. This positioning suggests potential steric interference within catalytically relevant regions; however, no conclusions regarding inhibitory activity can be drawn from docking alone. Consequently, Hispidin was retained for further structural analysis.

To prioritize candidates for more detailed interaction analysis, an empirical cutoff value of ≤ -8.0 kcal/mol was applied, as shown in Table 2. Ligand-receptor combinations meeting this criterion were selected for PLIP-based interaction profiling. This additional analysis enabled examination of hydrogen-bonding networks, hydrophobic contacts, π-π interactions, and other noncovalent interactions within predicted binding regions. While favorable docking scores may indicate stable predicted binding poses, they should not be interpreted as evidence of inhibitory activity. Rather, these results were used to support comparative structural analysis and hypothesis generation. Pulvinic acid, Pseurotin A, Hispidin, and Scytalone consistently demonstrated favorable docking characteristics and were therefore selected for further investigation. These fungal-derived metabolites may serve as useful structural scaffolds for future biochemical studies involving NDM-family metallo-β-lactamases.

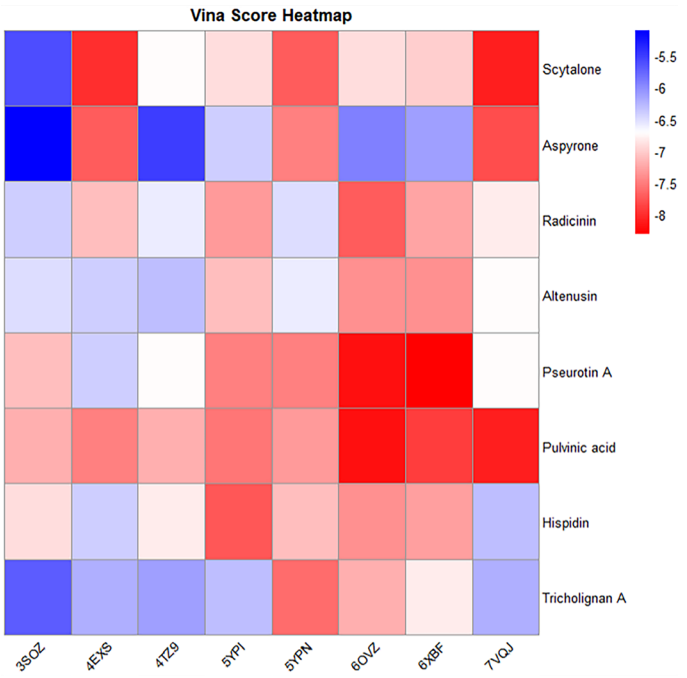


***Figure 2.*** *CB-Dock2 Vina score heatmap showing predicted binding affinities of fungal-derived compounds to NDM-family metallo-β-lactamases.*

***Table 2.*** *Shortlist for protein-ligand interaction profiling.*

| Receptor | PubChem CID | Ligand name | Vina Score |
|---|---|---|---|
| 6OVZ | 54682513 | Pulvinic acid | -9.2 |
| 6XBF | 9845622 | Pseurotin A | -9.0 |
| 6XBF | 54682513 | Pulvinic acid | -8.6 |
| 5YPI | 54685921 | Hispidin | -8.4 |
| 6OVZ | 9845622 | Pseurotin A | -8.3 |
| 7VQJ | 162567 | Scytalone | -8.1 |
| 7VQJ | 54682513 | Pulvinic acid | -8.1 |
| 4EXS | 162567 | Scytalone | -8.0 |

The receptor panel consisted of eight experimentally resolved NDM-family metallo-β-lactamase structures representing different ligand-bound states and conformational environments. This approach enabled comparative evaluation of fungal metabolite interactions across multiple structural states of NDM enzymes. Pulvinic acid is a biphenyl-like fungal pigment that has been investigated for antioxidant and antimicrobial properties in pulvinic acid-type mushroom pigments and related derivatives (28). Pseurotin A is a spirocyclic fungal metabolite that has been reported to exhibit mild antimicrobial activity and modulate immune-related enzymes and signaling pathways (29). Hispidin is a fungal polyketide known for antioxidant and antimicrobial activities (30). Scytalone is an intermediate in fungal melanin biosynthesis and has been investigated as a potential target for disrupting melanin production (31).

Each receptor structure was visualized in UCSF Chimera, highlighting the catalytic $Zn^{2+}$ ions and surrounding active-site residues (shown in green). Together, these experimentally resolved NDM-family metallo-β-lactamase structures provided a comparative framework for docking analysis and structural interpretation of fungal metabolite binding.

## Protein-Ligand Interaction Profiling

Understanding the structural features surrounding the catalytic center of NDM-family metallo-β-lactamases is important for interpreting docking and PLIP results. These enzymes utilize a dinuclear $Zn^{2+}$ catalytic center to hydrolyze β-lactam antibiotics. Because molecular docking provides static structural models, docking poses were interpreted as comparative structural observations rather than evidence of functional inhibition.

To provide structural context for docking interpretation, known β-lactamase inhibitors were included as reference ligands (Figure 3). Reference

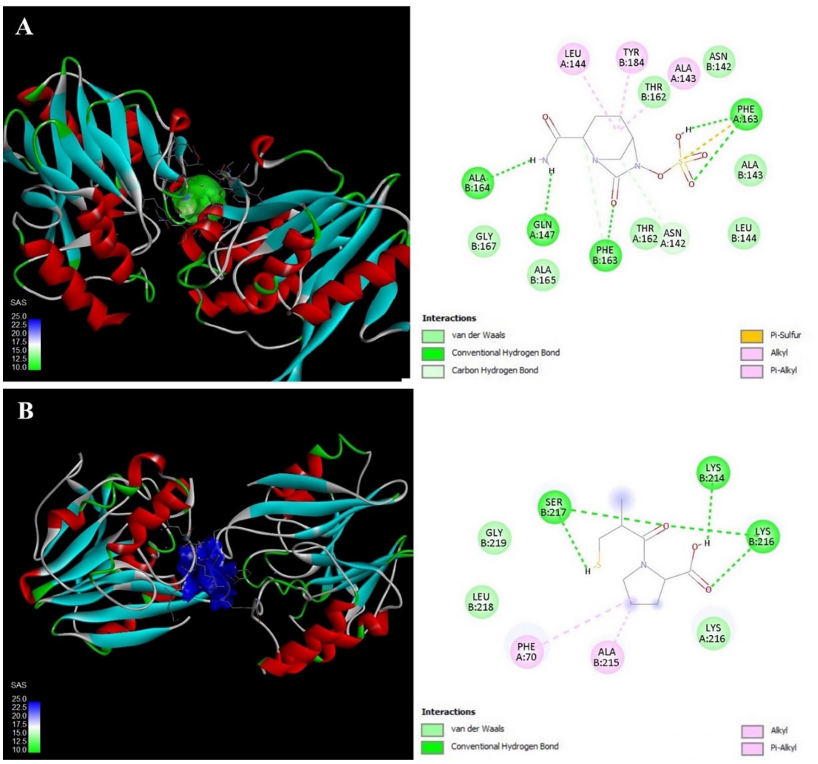


***Figure 3.*** *Docking poses of reference β-lactamase inhibitors in representative NDM-family metallo-β-lactamase structures. (A) Docking pose of avibactam in the NDM-family metallo-β-lactamase structure (PDB: 7VQJ), showing localization within the predicted binding region and interactions with surrounding residues. (B) Docking pose of captopril in the NDM-1 structure (PDB: 3S0Z), where the ligand localizes near the catalytic region and forms hydrogen-bond interactions, although no direct $Zn^{2+}$ coordination was observed in the predicted pose. Corresponding 2D interaction diagrams are shown on the right. These reference ligands were included to provide structural context for interpreting docking poses and protein–ligand interaction patterns.*

ligands provided a baseline for evaluating docking poses and interaction patterns. In the NDM-1 structure represented by PDB ID 3S0Z, captopril localized near the catalytic region and formed hydrogen-bond interactions with residues including Ser217, Lys216, and Lys214. However, direct $Zn^{2+}$ coordination was not observed in the predicted docking pose. Compared with the reference ligands, fungal metabolites exhibited more diverse binding modes, including localization near catalytically relevant regions and interactions within substrate-entry pathways. These observations highlight the structural diversity of the fungal metabolites while also emphasizing the limitations of docking-based interpretation. The catalytic center of NDM-family metallo-β-lactamases is formed by conserved metal-coordinating residues. Zn1 is coordinated by His120, His122, and His189, whereas Zn2 is coordinated by Asp124, Cys208, and His250 (34, 35). These residues directly coordinate the catalytic $Zn^{2+}$ ions and are essential for β-lactam hydrolysis. In addition to the metal-binding residues, neighboring amino acids contribute to substrate recognition and maintenance of the active-site architecture. Consequently, ligand interactions occurring near these regions may provide useful structural information regarding accessibility to catalytically relevant regions of the enzyme.

To better interpret protein-ligand interactions, general geometric criteria were considered (33). Hydrogen bonds with distances of approximately 2.5-3.2 Å and bond angles greater than 120° were regarded as potentially favorable. Salt bridges were considered relevant when oppositely charged groups were separated by less than 4 Å. For π-π interactions, distances of approximately 3.3-4.0 Å with appropriate ring orientations were considered favorable. Hydrophobic contacts were evaluated when nonpolar residues were located within approximately 4-5 Å of one another (25). These criteria provided structural context for interpreting the predicted interactions.

Docking and PLIP analyses demonstrated that fungal metabolites interacted with NDM-family metallo-β-lactamases through several distinct binding patterns (Figure 4). Visualization using solvent-accessible surface models and two-dimensional interaction maps facilitated examination of hydrogen-bonding networks, hydrophobic contacts, π-type interactions, and ligand localization relative to catalytically relevant regions (Supplemental Document 1). Individual docking poses were further examined using UCSF Chimera to support structural interpretation (Figure 5).

In the Zn-bound 5YPI structure, Hispidin was localized near the catalytic region. PLIP analysis identified hydrogen-bond interactions with Asn220 and Asp124, as well as interactions involving His122 and

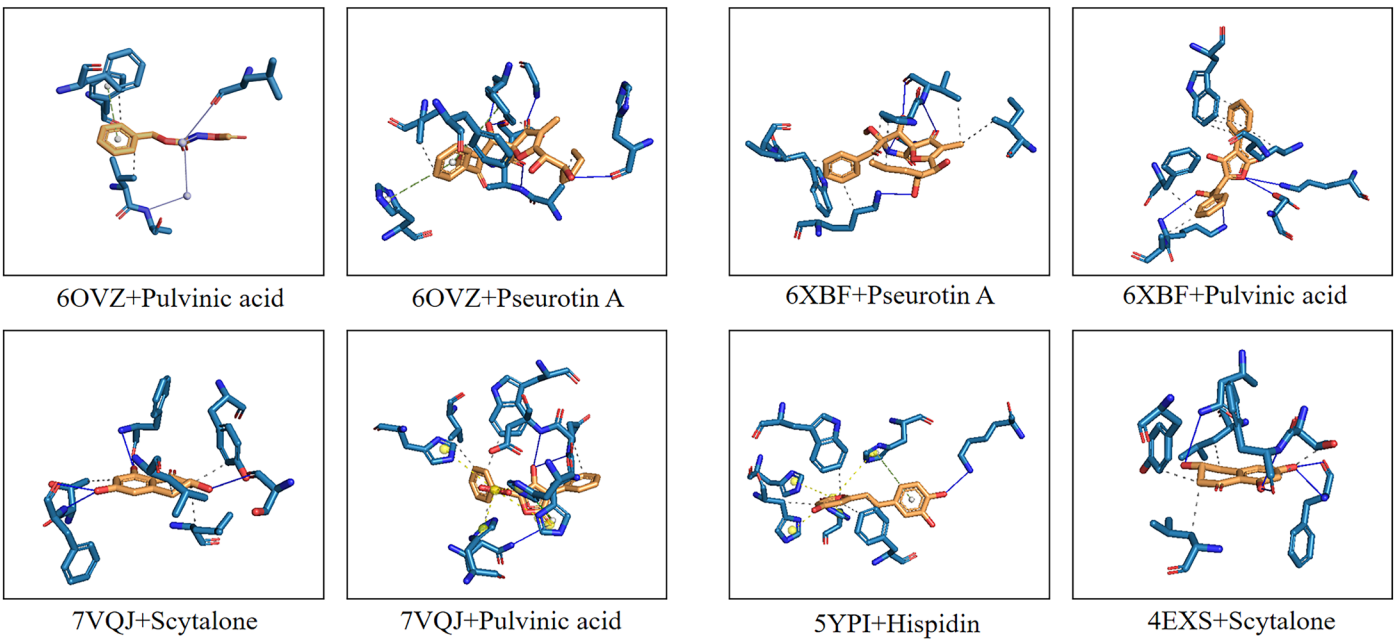


***Figure 4.*** *Representative top-ranked docking poses of fungal-derived metabolites bound to NDM-family metallo-β-lactamase structures from PLIP.*

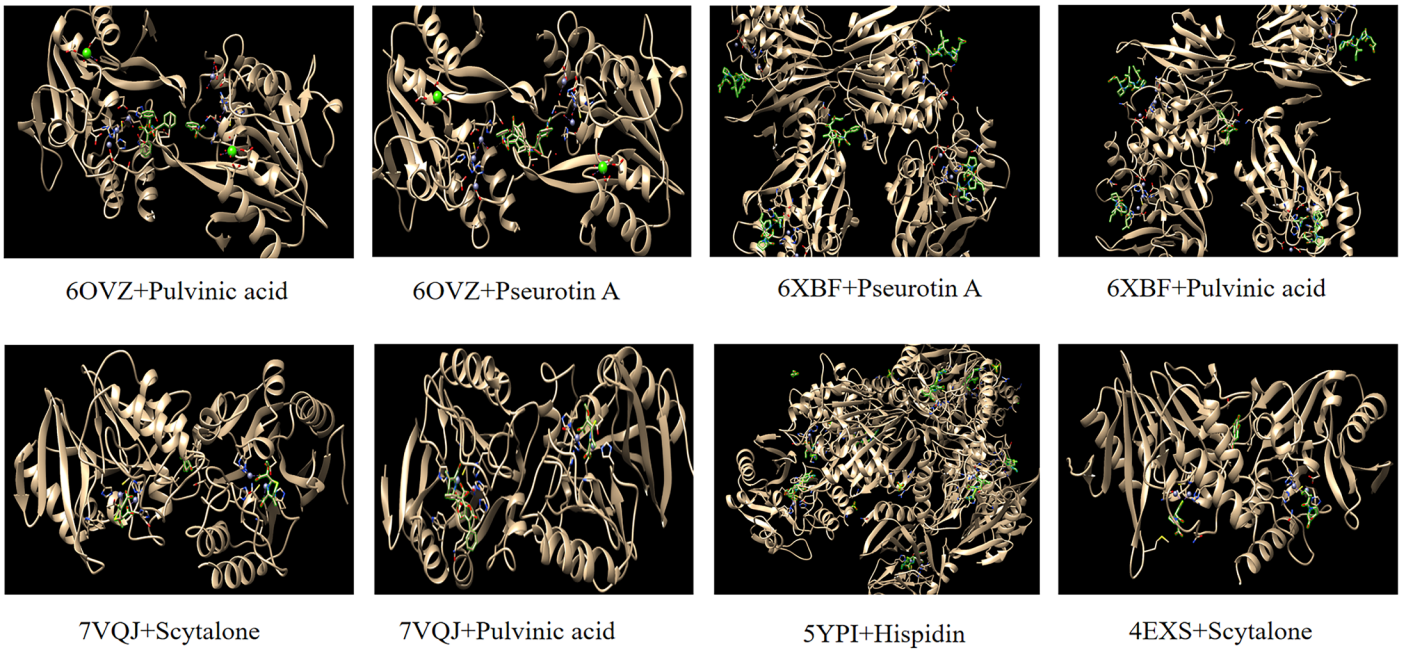


***Figure 5.*** *Representative top-ranked docking poses of fungal-derived metabolites bound to NDM-family metallo-β-lactamase structures. Green indicates the ligand.*

His250, residues associated with $Zn^{2+}$ coordination. Additional π-π interactions with Phe70 and Trp93 were observed. Although direct coordination with the catalytic $Zn^{2+}$ ions was not detected, the proximity of Hispidin to catalytically relevant residues justified its inclusion in subsequent structural analyses.

Scytalone exhibited a distinct binding mode in the 4EXS structure. The ligand was positioned within the substrate-binding region and formed hydrogen-bond and hydrophobic interactions with residues including Phe163, Asn142, Leu144, Tyr184, and Thr162. These residues contribute to the structural architecture of the substrate-recognition region. While direct $Zn^{2+}$ coordination was not observed, the predicted pose suggests that Scytalone occupies a region relevant to substrate access and recognition (Figure 6).

Pulvinic acid displayed a different binding pattern, localizing near the substrate-entry region rather than within the Zn-centered catalytic core. In the NDM-1 structure 6XBF, interactions were observed with Lys106, Trp168, Lys181, Lys242, and Gly219. Similar interaction patterns were observed in structures 6OVZ and 7VQJ, where Pulvinic acid interacted with residues including Ile105, Pro112, Val113, Trp168, Val169, Ser217, and Ser249. Notably, direct interactions with Zn-coordinating residues were not detected. These observations suggest a consistent tendency for Pulvinic acid to localize near substrate-access regions rather than the catalytic metal center.

Pseurotin A exhibited a similar binding pattern in the 6XBF structure. Predicted interactions primarily involved Ile105, Pro112, Val113, and Val169, residues located near the entrance of the active-site region. Direct interactions with Zn-coordinating residues were not observed.

Overall, none of the analyzed ligands demonstrated direct $Zn^{2+}$ coordination according to PLIP analysis. Instead, the compounds interacted with residues associated with active-site architecture or substrate-access regions. Consequently, the observed docking poses are more consistent with localization within catalytically relevant regions than with classical metal-chelation mechanisms. However, these observations are based solely on static docking models and should not be interpreted as evidence of functional inhibition. Collectively, these findings provide structural hypotheses that may guide future biochemical, biophysical, and experimental investigations of fungal-derived metabolites against NDM-family metallo-β-lactamases.

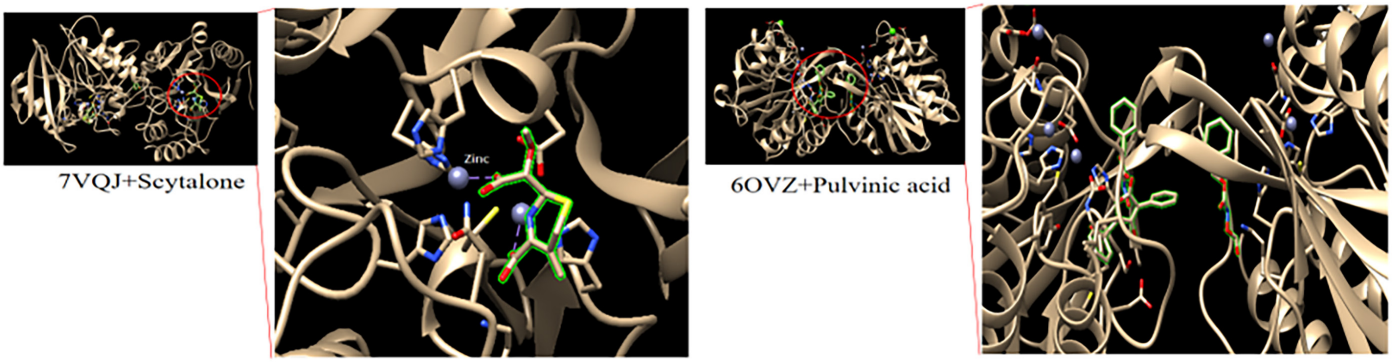


***Figure 6.*** *Representative docking poses of Scytalone (left) and Pulvinic acid (right) in NDM-family metallo-β-lactamase structures 7VQJ and 6OVZ, respectively. Scytalone was localized in close proximity to the Zn1-Zn2 catalytic region and interacted with residues surrounding the metal-binding site without direct $Zn^{2+}$ coordination. In contrast, Pulvinic acid was localized within the substrate-access region and positioned away from the catalytic metal center. The red circles indicate the predicted ligand-binding locations, and the enlarged views illustrate the spatial relationship between each ligand and the catalytic $Zn^{2+}$ ions. All structures were visualized using UCSF Chimera.*

**Drug-Likeness and Admet Profiles of Lead Fungal Metabolites**

To complement the docking and protein-ligand interaction analyses, four fungal metabolites (Pulvinic acid, Hispidin, Pseurotin A, and Scytalone) were evaluated for drug-likeness and ADMET-related properties using SwissADME (Supplemental Document 2). In addition to favorable structural interactions, potential lead compounds should possess physicochemical and pharmacokinetic characteristics compatible with further development. The BOILED-Egg model was used to predict human intestinal absorption (HIA) and blood-brain barrier (BBB) permeability. Red markers indicate compounds predicted to be non-substrates of P-glycoprotein (PGP-), whereas blue markers indicate predicted P-glycoprotein substrates (PGP+) (27). PAINS and Brenk filters were applied to identify structural features that may be associated with experimental interference or undesirable chemical reactivity (36). Lipinski's Rule of Five was used as a general indicator of drug-like properties (37). Supplemental Document 2 summarizes the predicted ADMET properties, physicochemical parameters, drug-likeness characteristics, and BOILED-Egg model outputs for Hispidin, Pseurotin A, Scytalone, and Pulvinic acid.

Scytalone exhibited favorable predicted pharmacokinetic properties, including high intestinal absorption, good aqueous solubility, and lack of predicted BBB permeability. In the BOILED-Egg model, Scytalone appeared as a red marker within the white region, consistent with favorable intestinal absorption and absence of P-glycoprotein-mediated efflux. No PAINS or Brenk alerts were identified, and the compound satisfied Lipinski's Rule of Five. Scytalone also displayed the lowest synthetic complexity among the compounds evaluated. Although its docking scores were less favorable than those of Pulvinic acid and Pseurotin A, its overall physicochemical and drug-likeness profile suggests that it may warrant further investigation.

Hispidin demonstrated high predicted intestinal absorption, favorable aqueous solubility, and limited BBB permeability. In the BOILED-Egg model, Hispidin appeared as a red marker within the white region, indicating favorable absorption characteristics and absence of predicted P-glycoprotein efflux. Although no PAINS alerts were detected, one Brenk alert associated with a catechol moiety was identified. Nevertheless, Hispidin satisfied Lipinski's Rule of Five and exhibited favorable predicted bioavailability. Combined with its localization near catalytically relevant regions in the docking analysis, these properties suggest that Hispidin may represent a useful scaffold for future optimization studies.

Pulvinic acid exhibited high predicted intestinal absorption and moderate aqueous solubility. Its calculated lipophilicity (LogP ≈ 2.4) is consistent with favorable membrane permeability. In the BOILED-Egg model, Pulvinic acid appeared as a red marker within the white region, indicating favorable absorption characteristics and absence of predicted P-glycoprotein efflux. No

PAINS alerts were detected; however, one Brenk alert associated with a Michael acceptor moiety was identified. Pulvinic acid also satisfied Lipinski's Rule of Five. Considering its favorable docking performance and acceptable predicted pharmacokinetic profile, Pulvinic acid may serve as a useful structural scaffold for future biochemical evaluation.

Pseurotin A exhibited favorable docking scores but less favorable predicted pharmacokinetic properties. The compound showed lower predicted intestinal absorption, relatively high molecular weight, and elevated topological polar surface area (TPSA), characteristics generally associated with reduced membrane permeability. In the BOILED-Egg model, Pseurotin A appeared as a blue marker near or outside the absorption region, indicating predicted P-glycoprotein efflux and limited absorption. In addition, both PAINS and Brenk alerts were identified, suggesting the presence of structural features that may complicate further development. Consequently, despite favorable docking characteristics, additional optimization would likely be required before considering Pseurotin A for future development.

### Limitations

Several limitations should be considered when interpreting the findings of this study. First, none of the analyzed compounds demonstrated direct coordination with the catalytic $Zn^{2+}$ ions based on docking and PLIP analyses. Although compounds such as Hispidin and Scytalone were localized near catalytically relevant regions, direct metal coordination was not observed. Similarly, Pulvinic acid and Pseurotin A were primarily localized near substrate-access regions rather than the catalytic metal center. Consequently, the proposed interaction patterns should be interpreted as structural observations rather than evidence of a specific inhibitory mechanism. Second, all findings were derived from computational analyses. Although molecular docking and interaction profiling are useful for identifying potential ligand-protein interactions, they cannot establish functional inhibition or biological activity. Experimental validation is therefore required to determine whether the predicted interactions are biologically relevant.

Third, the study evaluated only a limited number of fungal metabolites and NDM-family metallo-β-lactamase structures. Additional natural products, structural analogs, and NDM variants may exhibit different interaction patterns that were not captured in the present analysis. Fourth, important biological factors influencing drug performance, including solubility, toxicity, metabolic stability, and cellular uptake, were not experimentally evaluated. Although computational ADMET predictions were performed, these predictions should not be considered substitutes for experimental pharmacological assessment. Finally, molecular dynamics simulations, consensus scoring approaches, and binding free-energy calculations (e.g., MM/PBSA) were not performed. As a result, the stability and energetic reliability of the predicted docking poses could not be assessed. Therefore, the reported interactions should be regarded as preliminary structural hypotheses rather than confirmed binding modes. Taken together, these limitations indicate that the present work should be viewed as an exploratory computational screening study. Additional computational and experimental investigations will be necessary to evaluate the biological relevance of the observed interactions.

## CONCLUSION

This study employed a structure-based computational approach to investigate the interactions of fungal-derived metabolites with NDM-family metallo-β-lactamases. Molecular docking and protein-ligand interaction analyses identified four compounds, Hispidin, Scytalone, Pulvinic acid, and Pseurotin A, that exhibited relatively favorable docking scores ($\leq$ -8.0 kcal/mol) and distinct interaction patterns across multiple NDM-family receptor structures. Hispidin and Scytalone were frequently localized near catalytically relevant regions of NDM-family enzymes, whereas Pulvinic acid and Pseurotin A were more commonly observed near substrate-access regions. However, none of the analyzed compounds demonstrated direct $Zn^{2+}$ coordination. Consequently, the observed docking poses should be interpreted as structural hypotheses regarding potential ligand positioning rather than evidence of functional inhibition. ADMET predictions suggested that Hispidin and Scytalone possess relatively favorable drug-like characteristics, whereas Pulvinic acid and Pseurotin A may serve as structurally diverse scaffolds for future optimization efforts. Collectively, these findings highlight fungal-derived natural products as a source of chemically diverse scaffolds capable of interacting with NDM-family metallo-β-lactamase structures. Future studies should incorporate molecular dynamics simulations, binding free-energy calculations, and experimental validation, including enzymatic inhibition assays and substrate-competition experiments, to evaluate the stability and biological relevance of the predicted interactions. Such

investigations will be necessary to determine whether the identified compounds warrant further development as potential modulators of NDM-family metallo-β-lactamases.

## ACKNOWLEDGEMENT

This work was conducted as part of the North Carolina Regional 5 and State Science Fair. The project was completed independently, and no external editorial, technical, or analytical assistance was received. The author would like to thank the science fair judges for their valuable discussions and comments, which helped me improve and refine this work.

## CONFLICT OF INTEREST

The author declares that there are no conflicts of interest related to this work.

## REFERENCES

1. Cho H, Uehara T & Bernhardt TG. Beta-lactam antibiotics induce a lethal malfunctioning of the bacterial cell wall synthesis machinery. *Cell*. 2014; 159 (6): 1300-1311. https://doi.org/10.1016/j.cell.2014.11.017
2. Narendrakumar L, Chakraborty M, Kumari S, Paul D & Das B. β-Lactam potentiators to re-sensitize resistant pathogens: Discovery, development, clinical use and the way forward. *Frontiers in Microbiology.* 2023; 13: 1092556. https://doi.org/10.3389/fmicb.2022.1092556
3. Mora-Ochomogo M & Lohans CT. β-Lactam antibiotic targets and resistance mechanisms: from covalent inhibitors to substrates. RSC Medicinal Chemistry. 2021; 12 (10): 1623-1639. https://doi.org/10.1039/D1MD00200G
4. Bose P, Rangnekar A & Desikan P. NDM-beta-lactamase-1: Where do we stand?. *Indian Journal of Medical Research*. 2022; 155 (2): 243-252. https://doi.org/10.4103/ijmr.IJMR_685_19
5. CDC, 2025, CDC Report Finds Sharp Rise in Dangerous Drug-Resistant Bacteria. CDC Newsroom. https://www.cdc.gov/media/releases/2025/2025-cdc-report-finds-sharp-rise-in-dangerous-drug-resistant-bacteria.html (accessed on 2026-05-29)
6. Global Biodefense Staff. (2025, September 26). Rising threat of NDM-CRE in U.S. healthcare: CDC data reveal a concerning shift. Global Biodefense. https://globalbiodefense.com/2025/09/26/cdc-ndm-cre-surge-drug-resistant-bacteria-2025/ (accessed on 2026-05-29)
7. Logan LK & Weinstein RA. The epidemiology of carbapenem-resistant Enterobacteriaceae: the impact and evolution of a global menace. *The Journal of infectious diseases.* 2017; 215 (suppl_1): S28-S36. https://doi.org/10.1093/infdis/jiw282
8. Alvisi G, Curtoni A, Fonnesu R, Piazza A, Signoretto, C, Piccinini G, *et al*. Epidemiology and genetic traits of carbapenemase-producing enterobacterales: A global threat to human health. *Antibiotics*. 2025; 14 (2): 141. https://doi.org/10.3390/antibiotics14020141
9. Thomas CA, Cheng Z. Bethel CR, Hujer AM, Sturgill AM, Onuoha K, *et al*. The directed evolution of NDM-1. *Antimicrobial Agents and Chemotherapy*. 2023; 67 (11): e00714-23. https://doi.org/10.1128/aac.00714-23
10. Karaiskos I, Galani I, Daikos GL & Giamarellou H. Breaking through resistance: A comparative review of new beta-lactamase inhibitors (Avibactam, vaborbactam, relebactam) against multidrug-resistant superbugs. Antibiotics. 2025; 14 (5): 528. https://doi.org/10.3390/antibiotics14050528
11. Nahar L, Hagiya H, Gotoh K, Asaduzzaman M & Otsuka F. New Delhi metallo-beta-lactamase inhibitors: a systematic scoping review. Journal of Clinical Medicine. 2024; 13 (14): 4199. https://doi.org/10.3390/jcm13144199
12. Wang T, Xu K, Zhao L, Tong R, Xiong L & Shi J. Recent research and development of NDM-1 inhibitors. European journal of medicinal chemistry. 2021; 223: 113667. https://doi.org/10.1016/j.ejmech.2021.113667
13. Li X, Zhao J, Zhang B, Duan X, Jiao J, Wu W, *et al*. Drug development concerning metallo-β-lactamases in gram-negative bacteria. *Frontiers in Microbiology.* 2022; 13: 959107. https://doi.org/10.3389/fmicb.2022.959107
14. Keller NP. Fungal secondary metabolism: regulation, function and drug discovery. *Nature Reviews Microbiology.* 2019; 17 (3): 167-180. https://doi.org/10.1038/s41579-018-0121-1
15. Bills GF & Gloer JB. Biologically active secondary metabolites from the fungi. *Microbiology spectrum*. 2016; 4 (6): 10-1128. https://doi.org/10.1128/microbiolspec.funk-0009-2016
16. Tessema FB, Asfaw TB, Tadesse MG, Gonfa YH & Bachheti RK. In silico studies as support for natural products research. *Medinformatics*. 2025; 2 (1): 11-21. https://doi.org/10.47852/bonviewMEDIN42023842
17. RCSB Protein Data Bank (RCSB PDB). https://www.rcsb.org/ (accessed on 2026-05-29)
18. Pettersen EF, Goddard TD, Huang CC, Couch GS, Greenblatt DM, Meng EC, *et al*. UCSF Chimera—a visualization system for exploratory research and analysis. *Journal of computational chemistry*. 2004; 25 (13): 1605-1612. https://doi.org/10.1002/jcc.20084

19. Liu Y, Yang X, Gan J, Chen S, Xiao ZX & Cao Y. CB-Dock2: improved protein-ligand blind docking by integrating cavity detection, docking and homologous template fitting. *Nucleic acids research*. 2022; 50 (W1): W159-W164. https://doi.org/10.1093/nar/gkac394
20. European Bioinformatics Institute (EMBL-EBI). ChEBI. https://www.ebi.ac.uk/chebi/ (accessed on 2026-05-29)
21. LOTUS Natural Products Online Database. https://lotus.naturalproducts.net/ (accessed on 2026-05-29)
22. National Center for Biotechnology Information (NCBI). PubChem. https://pubchem.ncbi.nlm.nih.gov/
23. Cao Lab. CB-Dock2 web server. http://183.56.231.194:8001/cb-dock2/index.php (accessed on 2026-05-29)
24. Technische Universität Dresden. Protein-Ligand Interaction Profiler (PLIP). https://plip-tool.biotec.tu-dresden.de/plip-web/plip (accessed on 2026-05-29)
25. Schake P, Bolz SN, Linnemann K & Schroeder M. PLIP 2025: introducing protein-protein interactions to the protein-ligand interaction profiler. *Nucleic acids research*. 2025; 53 (W1): W463-W465. https://doi.org/10.1093/nar/gkaf361
26. Swiss Institute of Bioinformatics (SIB). SwissADME. http://www.swissadme.ch/ (accessed on 2026-05-29)
27. Daina A & Zoete V. A boiled-egg to predict gastrointestinal absorption and brain penetration of small molecules. *ChemMedChem*. 2016; 11 (11): 1117-1121. https://doi.org/10.1002/cmdc.201600182
28. Karunarathna SC, Tibpromma S, Lu W, Perera H, Tarafder E, Karunarathna BS, *et al*. Basidiomycete pigments as sustainable food colorants and stabilizers: from fungal biology to industrial potential. Frontiers in Microbiology. 2025; 16: 1725536. https://doi.org/10.3389/fmicb.2025.1725536
29. Vasicek O, Rubanova D, Chytkova B & Kubala L. Natural pseurotins inhibit proliferation and inflammatory responses through the inactivation of STAT signaling pathways in macrophages. *Food and Chemical Toxicology*. 2020; 141: 111348. https://doi.org/10.1016/j.fct.2020.111348
30. Palkina KA, Ipatova DA, Shakhova ES, Balakireva AV & Markina NM. Therapeutic potential of hispidin—fungal and plant polyketide. *Journal of Fungi*. 2021; 7 (5): 323. https://doi.org/10.3390/jof7050323
31. Motoyama T, Kondoh Y, Shimizu T, Hayashi T, Honda K, Uchida M, *et al*. Identification of scytalone dehydratase inhibitors effective against melanin biosynthesis dehydratase inhibitor-resistant pyricularia oryzae. *Journal of Agricultural and Food Chemistry*. 2022; 70 (10): 3109-3116. https://doi.org/10.1021/acs.jafc.1c04984
32. Bahr G, Gonzalez LJ & Vila AJ. Metallo-β-lactamases in the age of multidrug resistance: from structure and mechanism to evolution, dissemination, and inhibitor design. *Chemical reviews*. 2021; 121 (13): 7957-8094. https://doi.org/10.1021/acs.chemrev.1c00138
33. De Freitas RF & Schapira M. A systematic analysis of atomic protein-ligand interactions in the PDB. *Medchemcomm*. 2017; 8 (10): 1970-1981. https://doi.org/10.1039/C7MD00381A
34. Zhang G & Hao Q. Crystal structure of NDM-1 reveals a common β-lactam hydrolysis mechanism. *The FASEB Journal*. 2011; 25 (8): 2574-2582. https://doi.org/10.1096/fj.11-184036
35. Palzkill T. Metallo-β-lactamase structure and function. *Annals of the New York Academy of Sciences*. 2013; 1277 (1): 91-104. https://doi.org/10.1111/j.1749-6632.2012.06796.
36. Baell JB & Holloway GA. New substructure filters for removal of pan assay interference compounds (PAINS) from screening libraries and for their exclusion in bioassays. *Journal of medicinal chemistry*. 2010; 53 (7): 2719-2740. https://doi.org/10.1021/jm901137j
37. Lipinski CA. Lead-and drug-like compounds: the rule-of-five revolution. Drug discovery today: *Technologies*. 2004; 1 (4): 337-341. https://doi.org/10.1016/j.ddtec.2004.11.007

## SUPPLEMENTAL TABLES AND FIGURES

***Supplemental Table 1.*** *Fungal-derived natural compounds selected for molecular docking against β-lactamases.*

| PubChem CID | Compound Name | Molecular Formula | Molecular Weight (g/mol) | Source Organisms | Primary Hazards |
|---|---|---|---|---|---|
| 6303 | Cordycepin | $C_{10}H_{13}N_5O_3$ | 251.24 | Cordyceps militaris | Acute toxic, Irritant |
| 72537 | Rubrofusarin | $C_{15}H_{12}O_5$ | 272.25 | Fusarium graminearum, Aspergillus niger | Irritant |
| 441140 | Griseofulvin | $C_{17}H_{17}ClO_6$ | 352.8 | Penicillium griseofulvum | Irritant, health hazard |
| 444679 | Ergosterol | $C_{28}H_{44}O$ | 396.6 | Agaricus blazei, Gymnopilus spectabilis | Acute toxic |
| 446541 | Mycophenolic Acid | $C_{17}H_{20}O_6$ | 320.3 | Penicillium brevicompactum, P. stoloniferum, P. echinulatum | Irritant, health hazard, Environmental hazard |
| 6438437 | Chaetoglobosin | $C_{32}H_{36}N_2O_5$ | 528.6 | Chaetomium subaffine, Cunila | Irritant |
| 6917655 | Fumagillin | $C_{26}H_{34}O_7$ | 458.5 | Aspergillus fumigatus | Irritant |
| 9929643 | Hypothemycin | $C_{19}H_{22}O_8$ | 378.4 | Aigialus parvus, Hypomyces subiculosus, | Irritant |
| 70697743 | Epichlicin | $C_{48}H_{74}N_{12}O_{14}$ | 1043.2 | Epichloe typhina | none (no 3D) |
| 162567 | Scytalone * | $C_{10}H_{10}O_4$ | 194.18 | Cytospora populina, Ceratocystis fimbriata | none |
| 167653 | Aspyrone* | $C_9H_{12}O_4$ | 184.19 | Aspergillusochraceus, Exophiala | none |
| 5381458 | Radicinin* | $C_{12}H_{12}O_5$ | 236.22 | Stemphylium radicinum | none |
| 6918469 | Altenusin* | $C_{15}H_{14}O_6$ | 290.27 | Alternaria, Penicillium simplicissimum, Talaromyces flavus, | none |
| 9845622 | Pseurotin A* | $C_{22}H_{25}NO_8$ | 431.4 | Aspergillus insulicola, Cordyceps tenuipes | none |
| 54682513 | Pulvinic acid* | $C_{18}H_{12}O_5$ | 308.3 | Candelaria concolor, Aspergillus terreus | none |
| 54685921 | Hispidin* | $C_{13}H_{10}O_5$ | 246.21 | Phellinus pomaceus, Gymnopilus spectabilis, | none |
| 162370967 | Tricholignan A* | $C_{13}H_{16}O_3$ | 220.26 | Ascomycota, Trichoderma harzianum | none |

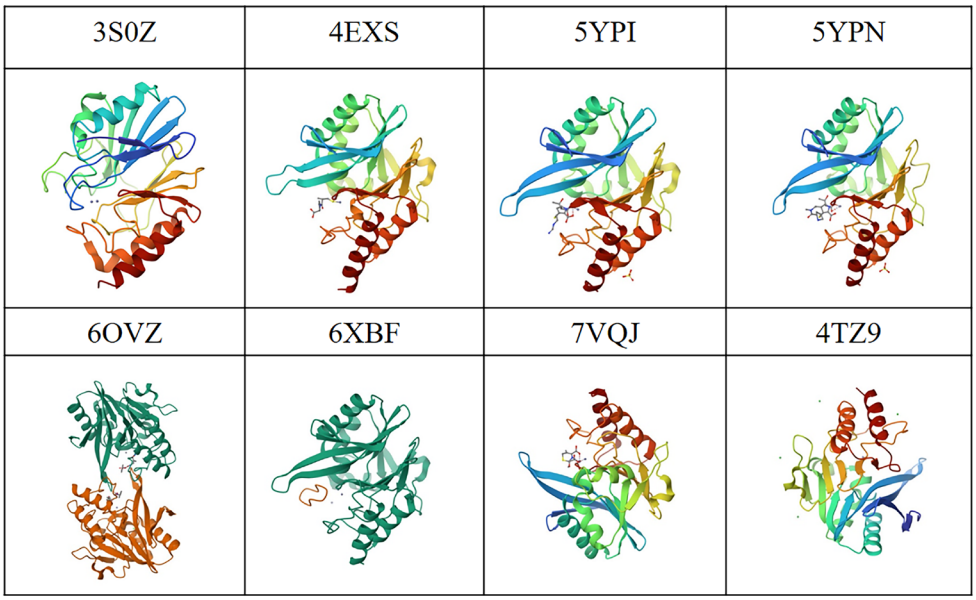


***Supplement Figure 1.*** *Three-dimensional structures of representative β-lactamase receptors used for molecular docking.*

***Supplemental Table 2. Molecular docking results of fungal-derived compounds against β-lactamase receptors.*** *Binding affinities (Vina scores), pocket IDs, and cavity properties for each ligand-receptor complex were obtained from CB-Dock2. Lower (more negative) Vina scores indicate stronger predicted binding affinities. All coordinates (center and docking box size) correspond to the identified binding cavities for each β-lactamase structure.*

| Protein (PDB ID) | Ligand | | Pocket ID | Vina Score (kcal/mol) | Cavity Volume (Å³) | Center | Docking size (x, y, z) |
|---|---|---|---|---|---|---|---|
| 3S0Z | 162567 | Scytalone | C2 | -5.6 | 385 | 9, 16, -2 | 18, 18, 18 |
| 3S0Z | 167653 | Aspyrone | C2 | -5.1 | 359 | 13, 15, -14 | 18, 18, 18 |
| 3S0Z | 5381458 | Radicinin | C1 | -6.4 | 385 | 9, 16, -2 | 19, 19, 19 |
| 3S0Z | 6918469 | Altenusin | C1 | -6.5 | 385 | 9, 16, -2 | 20, 20, 20 |
| 3S0Z | 9845622 | Pseurotin A | C1 | -7.1 | 385 | 9, 16, -2 | 21, 21, 21 |
| 3S0Z | 54682513 | Pulvinic acid | C2 | -7.2 | 359 | 13, 15, -14 | 21, 21, 21 |
| 3S0Z | 54685921 | Hispidin | C2 | -6.9 | 359 | 13, 15, -14 | 22, 22, 22 |
| 3S0Z | 162370967 | Tricholignan A | C2 | -5.7 | 359 | 13, 15, -14 | 20, 20, 20 |
| 4EXS | 162567 | Scytalone | C5 | -8 | 246 | -41, 23, -16 | 18, 18, 18 |
| 4EXS | 167653 | Aspyrone | C5 | -7.7 | 246 | -41, 23, -16 | 18, 18, 18 |
| 4EXS | 5381458 | Radicinin | C1 | -7.1 | 350 | -39, 3, -5 | 19, 19, 19 |
| 4EXS | 6918469 | Altenusin | C1 | -6.4 | 350 | -39, 3, -5 | 20, 20, 20 |
| 4EXS | 9845622 | Pseurotin A | C1 | -6.4 | 350 | -39, 3, -5 | 21, 21, 21 |
| 4EXS | 54682513 | Pulvinic acid | C1 | -7.5 | 350 | -39, 3, -5 | 21, 21, 21 |
| 4EXS | 54682513 | Pulvinic acid | C5 | -7.5 | 246 | -41, 23, -16 | 21, 21, 21 |
| 4EXS | 54685921 | Hispidin | C1 | -6.4 | 350 | -39, 3, -5 | 22, 22, 22 |
| 4EXS | 162370967 | Tricholignan A | C5 | -6.2 | 246 | -41, 23, -16 | 20, 20, 20 |

***Continued Supplemental Table 2. Molecular docking results of fungal-derived compounds against β-lactamase receptors.*** *Binding affinities (Vina scores), pocket IDs, and cavity properties for each ligand-receptor complex were obtained from CB-Dock2. Lower (more negative) Vina scores indicate stronger predicted binding affinities. All coordinates (center and docking box size) correspond to the identified binding cavities for each β-lactamase structure.*

| Protein (PDB ID) | Ligand | | Pocket ID | Vina Score (kcal/mol) | Cavity Volume (Å³) | Center | Docking size (x, y, z) |
|---|---|---|---|---|---|---|---|
| 4TZ9 | 162567 | Scytalone | C3 | -6.7 | 102 | 0, 34, -21 | 18, 18, 18 |
| 4TZ9 | 167653 | Aspyrone | C4 | -5.5 | 91 | -20, 35, -26 | 18, 18, 18 |
| 4TZ9 | 5381458 | Radicinin | C3 | -6.6 | 102 | 0, 34, -21 | 19, 19, 19 |
| 4TZ9 | 6918469 | Altenusin | C5 | -6.3 | 90 | 4, 27, -30 | 20, 20, 20 |
| 4TZ9 | 9845622 | Pseurotin A | C3 | -6.7 | 102 | 0, 34, -21 | 21, 21, 21 |
| 4TZ9 | 54682513 | Pulvinic acid | C1 | -7.2 | 259 | -20, 23, -23 | 21, 21, 21 |
| 4TZ9 | 54685921 | Hispidin | C3 | -6.8 | 102 | 0, 34, -21 | 22, 22, 22 |
| 4TZ9 | 54685921 | Hispidin | C5 | -6.8 | 90 | 4, 27, -30 | 22, 22, 22 |
| 4TZ9 | 162370967 | Tricholignan A | C3 | -6.1 | 102 | 0, 34, -21 | 20, 20, 20 |
| 5YPI | 162567 | Scytalone | C4 | -6.9 | 2577 | -34, -50, -33 | 18, 30, 27 |
| 5YPI | 167653 | Aspyrone | C4 | -6.4 | 2577 | -34, -50, -33 | 18, 30, 27 |
| 5YPI | 5381458 | Radicinin | C1 | -7.4 | 8664 | -38, -11, -10 | 35, 30, 35 |
| 5YPI | 5381458 | Radicinin | C5 | -7.4 | 1595 | -35, -12, -43 | 19, 30, 19 |
| 5YPI | 5381458 | Radicinin | C4 | -7.2 | 2577 | -34, -50, -33 | 19, 30, 27 |
| 5YPI | 6918469 | Altenusin | C5 | -7.2 | 1595 | -35, -12, -43 | 20, 30, 20 |
| 5YPI | 6918469 | Altenusin | C1 | -7 | 8664 | -38, -11, -10 | 35, 30, 35 |
| 5YPI | 9845622 | Pseurotin A | C1 | -7.6 | 8664 | -38, -11, -10 | 35, 30, 35 |
| 5YPI | 9845622 | Pseurotin A | C4 | -7.6 | 2577 | -34, -50, -33 | 21, 30, 27 |
| 5YPI | 9845622 | Pseurotin A | C5 | -7.5 | 1595 | -35, -12, -43 | 21, 30, 21 |
| 5YPI | 9845622 | Pseurotin A | C3 | -7.2 | 3914 | -50, -30, -23 | 29, 27, 33 |
| 5YPI | 54682513 | Pulvinic acid | C1 | -7.7 | 8664 | -38, -11, -10 | 35, 30, 35 |
| 5YPI | 54682513 | Pulvinic acid | C4 | -7.7 | 2577 | -34, -50, -33 | 21, 30, 27 |
| 5YPI | 54682513 | Pulvinic acid | C5 | -7.7 | 1595 | -35, -12, -43 | 21, 30, 21 |
| 5YPI | 54682513 | Pulvinic acid | C3 | -7.5 | 3914 | -50, -30, -23 | 29, 27, 33 |
| 5YPI | 54682513 | Pulvinic acid | C2 | -7.2 | 4653 | -15, -20, -26 | 21, 35, 31 |
| 5YPI | 54685921 | Hispidin | C1 | -8.4 | 8664 | -38, -11, -10 | 35, 30, 35 |
| 5YPI | 54685921 | Hispidin | C4 | -7.4 | 2577 | -34, -50, -33 | 22, 30, 22 |
| 5YPI | 54685921 | Hispidin | C5 | -7.4 | 1595 | -35, -12, -43 | 22, 30, 22 |
| 5YPI | 162370967 | Tricholignan A | C1 | -6.3 | 8664 | -38, -11, -10 | 35, 30, 35 |
| 5YPN | 162567 | Scytalone | C1 | -7.7 | 211 | -55, 91, 87 | 18, 18, 18 |
| 5YPN | 167653 | Aspyrone | C1 | -7.5 | 211 | -55, 91, 87 | 18, 18, 18 |
| 5YPN | 5381458 | Radicinin | C5 | -6.5 | 153 | -61, 99, 75 | 19, 19, 19 |
| 5YPN | 6918469 | Altenusin | C1 | -6.6 | 211 | -55, 91, 87 | 20, 20, 20 |

***Continued Supplemental Table 2. Molecular docking results of fungal-derived compounds against β-lactamase receptors.*** *Binding affinities (Vina scores), pocket IDs, and cavity properties for each ligand-receptor complex were obtained from CB-Dock2. Lower (more negative) Vina scores indicate stronger predicted binding affinities. All coordinates (center and docking box size) correspond to the identified binding cavities for each β-lactamase structure.*

| Protein (PDB ID) | Ligand | | Pocket ID | Vina Score (kcal/mol) | Cavity Volume (Å³) | Center | Docking size (x, y, z) |
|---|---|---|---|---|---|---|---|
| 5YPN | 9845622 | Pseurotin A | C4 | -7.5 | 157 | -40, 75, 95 | 21, 21, 21 |
| 5YPN | 54682513 | Pulvinic acid | C4 | -7.5 | 157 | -40, 75, 95 | 21, 21, 21 |
| 5YPN | 54682513 | Pulvinic acid | C1 | -7.3 | 211 | -55, 91, 87 | 21, 21, 21 |
| 5YPN | 54682513 | Pulvinic acid | C5 | -7.2 | 153 | -61, 99, 75 | 21, 21, 21 |
| 5YPN | 54685921 | Hispidin | C5 | -7.1 | 153 | -61, 99, 75 | 22, 22, 22 |
| 5YPN | 162370967 | Tricholignan A | C1 | -7.6 | 211 | -55, 91, 87 | 20, 20, 20 |
| 6OVZ | 162567 | Scytalone | C1 | -6.9 | 2170 | 4, -13, -35 | 18, 25, 28 |
| 6OVZ | 167653 | Aspyrone | C1 | -5.9 | 2170 | 4, -13, -35 | 18, 25, 28 |
| 6OVZ | 5381458 | Radicinin | C1 | -7.7 | 2170 | 4, -13, -35 | 19, 25, 28 |
| 6OVZ | 6918469 | Altenusin | C1 | -7.5 | 2170 | 4, -13, -35 | 20, 20, 28 |
| 6OVZ | 6918469 | Altenusin | C5 | -7.4 | 138 | 10, -19, -28 | 20, 20, 20 |
| 6OVZ | 6918469 | Altenusin | C3 | -7.3 | 152 | 13, -11, -33 | 20, 20, 20 |
| 6OVZ | 9845622 | Pseurotin A | C1 | -8.3 | 2170 | 4, -13, -35 | 21, 21, 28 |
| 6OVZ | 9845622 | Pseurotin A | C3 | -8.3 | 152 | 13, -11, -33 | 21, 21, 21 |
| 6OVZ | 9845622 | Pseurotin A | C5 | -8 | 138 | 10, -19, -28 | 21, 21, 21 |
| 6OVZ | 54682513 | Pulvinic acid | C1 | -9.2 | 2170 | 4, -13, -35 | 21, 21, 28 |
| 6OVZ | 54682513 | Pulvinic acid | C5 | -8.3 | 138 | 10, -19, -28 | 21, 21, 21 |
| 6OVZ | 54682513 | Pulvinic acid | C3 | -8.1 | 152 | 13, -11, -33 | 21, 21, 21 |
| 6OVZ | 54682513 | Pulvinic acid | C2 | -7.2 | 179 | 4, -25, -36 | 21, 21, 21 |
| 6OVZ | 54685921 | Hispidin | C1 | -7.7 | 2170 | 4, -13, -35 | 22, 22, 28 |
| 6OVZ | 54685921 | Hispidin | C5 | -7.5 | 138 | 10, -19, -28 | 22, 22, 22 |
| 6OVZ | 54685921 | Hispidin | C3 | -7.2 | 152 | 13, -11, -33 | 22, 22, 22 |
| 6OVZ | 54685921 | Hispidin | C2 | -7.1 | 179 | 4, -25, -36 | 22, 22, 22 |
| 6OVZ | 162370967 | Tricholignan A | C1 | -7.2 | 2170 | 4, -13, -35 | 20, 20, 28 |
| 6XBF | 162567 | Scytalone | C5 | -7 | 706 | -32, -49, 1 | 18, 18, 18 |
| 6XBF | 167653 | Aspyrone | C1 | -6.1 | 1947 | -42, -74, 2 | 26, 28, 18 |
| 6XBF | 5381458 | Radicinin | C5 | -7.4 | 706 | -32, -49, 1 | 19, 19, 19 |
| 6XBF | 5381458 | Radicinin | C1 | -7.2 | 1947 | -42, -74, 2 | 26, 28, 19 |
| 6XBF | 5381458 | Radicinin | C3 | -7.2 | 760 | -46, -66, -27 | 19, 19, 19 |
| 6XBF | 6918469 | Altenusin | C1 | -7.4 | 1947 | -42, -74, 2 | 26, 28, 20 |
| 6XBF | 6918469 | Altenusin | C5 | -7.4 | 706 | -32, -49, 1 | 20, 20, 20 |
| 6XBF | 9845622 | Pseurotin A | C1 | -9 | 1947 | -42, -74, 2 | 21, 28, 21 |
| 6XBF | 9845622 | Pseurotin A | C4 | -7.6 | 732 | -49, -94, -29 | 21, 21, 21 |

***Continued Supplemental Table 2. Molecular docking results of fungal-derived compounds against β-lactamase receptors.*** *Binding affinities (Vina scores), pocket IDs, and cavity properties for each ligand-receptor complex were obtained from CB-Dock2. Lower (more negative) Vina scores indicate stronger predicted binding affinities. All coordinates (center and docking box size) correspond to the identified binding cavities for each β-lactamase structure.*

| Protein (PDB ID) | Ligand | | Pocket ID | Vina Score (kcal/mol) | Cavity Volume (Å³) | Center | Docking size (x, y, z) |
|---|---|---|---|---|---|---|---|
| 6XBF | 54682513 | Pulvinic acid | C1 | -8.6 | 1947 | -42, -74, 2 | 21, 28, 21 |
| 6XBF | 54682513 | Pulvinic acid | C5 | -7.8 | 706 | -32, -49, 1 | 21, 21, 21 |
| 6XBF | 54682513 | Pulvinic acid | C3 | -7.3 | 760 | -46, -66, -27 | 21, 21, 21 |
| 6XBF | 54685921 | Hispidin | C1 | -7.6 | 1947 | -42, -74, 2 | 22, 28, 22 |
| 6XBF | 54685921 | Hispidin | C5 | -7.3 | 706 | -32, -49, 1 | 22, 22, 22 |
| 6XBF | 54685921 | Hispidin | C3 | -7 | 760 | -46, -66, -27 | 22, 22, 22 |
| 6XBF | 162370967 | Tricholignan A | C1 | -6.8 | 1947 | -42, -74, 2 | 26, 28, 20 |
| 7VQJ | 162567 | Scytalone | C3 | -8.1 | 279 | 21, 31, 14 | 18, 18, 18 |
| 7VQJ | 167653 | Aspyrone | C3 | -7.8 | 279 | 21, 31, 14 | 18, 18, 18 |
| 7VQJ | 5381458 | Radicinin | C5 | -6.8 | 167 | 19, 16, 29 | 19, 19, 19 |
| 7VQJ | 6918469 | Altenusin | C3 | -6.7 | 279 | 21, 31, 14 | 20, 20, 20 |
| 7VQJ | 9845622 | Pseurotin A | C5 | -6.7 | 167 | 19, 16, 29 | 21, 21, 21 |
| 7VQJ | 54682513 | Pulvinic acid | C5 | -8.1 | 167 | 19, 16, 29 | 21, 21, 21 |
| 7VQJ | 54685921 | Hispidin | C5 | -6.3 | 167 | 19, 16, 29 | 22, 22, 22 |
| 7VQJ | 162370967 | Tricholignan A | C3 | -6.2 | 279 | 21, 31, 14 | 20, 20, 20 |

***Supplemental Document 1.*** *Discovery Studio Visualizer representation of solvent-accessible surface (SAS) maps and 2D interaction diagrams for selected high-affinity fungal metabolites bound to carbapenemase active sites.*

| | | |
|---|---|---|
| 6OVZ_Pulvinic acid | 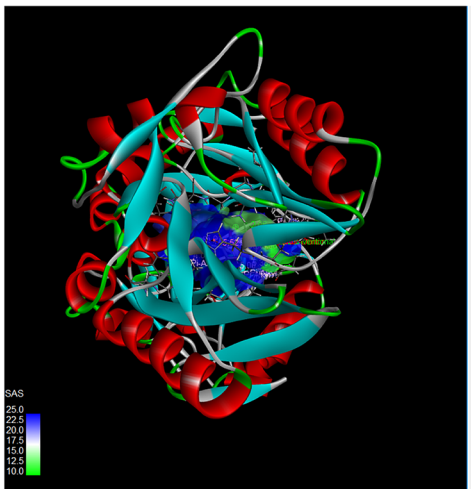  | 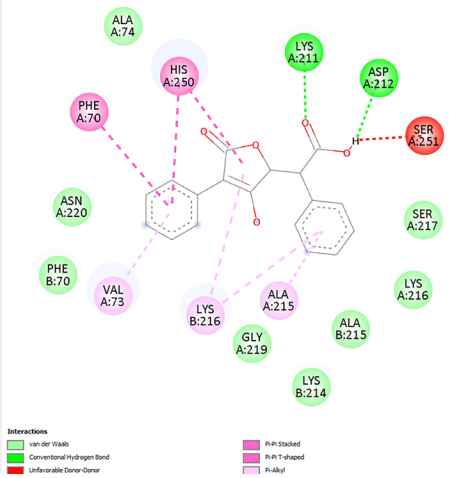  |
| 6XBF_Pseurotin A | 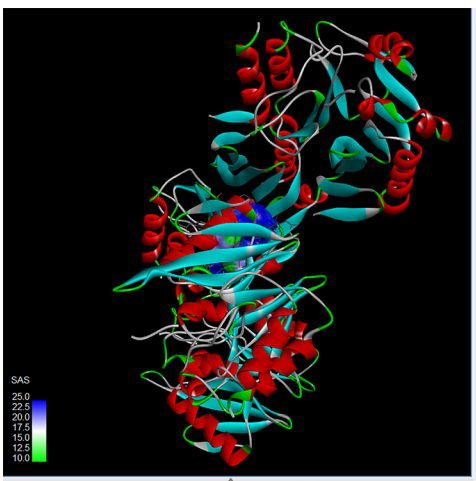  | 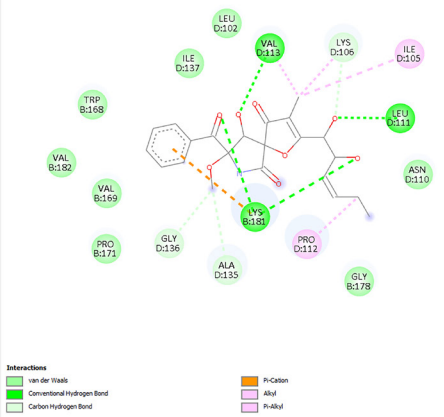  |
| 6XBF_Pulvinic acid | 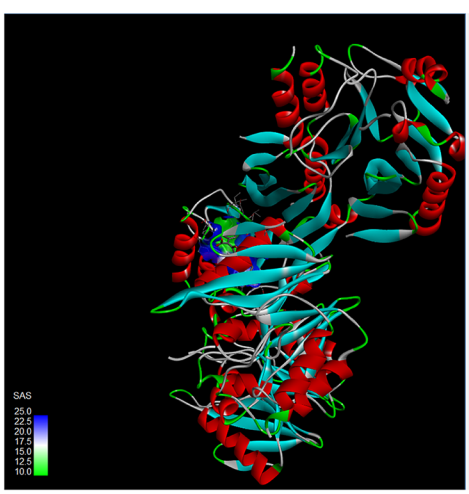  | 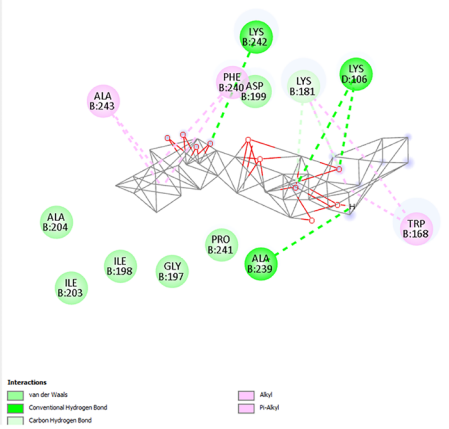  |

***Continued Supplemental Document 1.*** *Discovery Studio Visualizer representation of solvent-accessible surface (SAS) maps and 2D interaction diagrams for selected high-affinity fungal metabolites bound to carbapenemase active sites.*

| | |
|---|---|
| 5YPI_Hispidin | 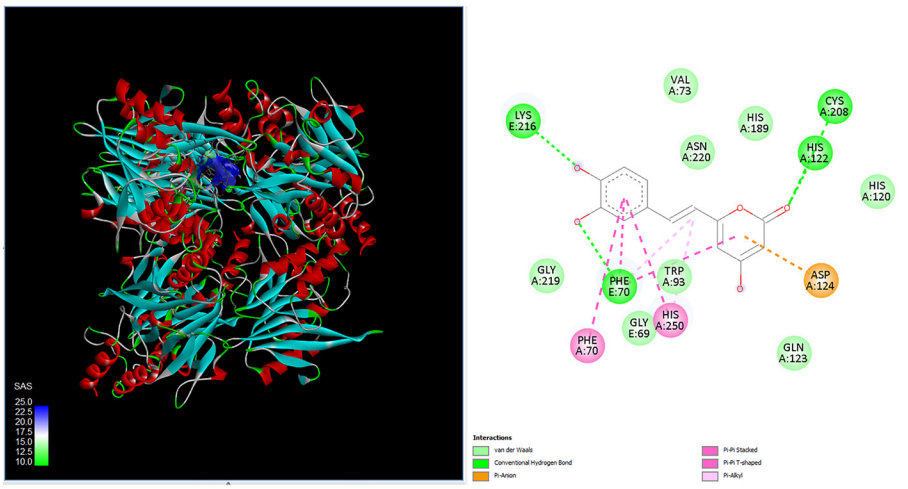 |
| 6OVZ_Pseurotin A | 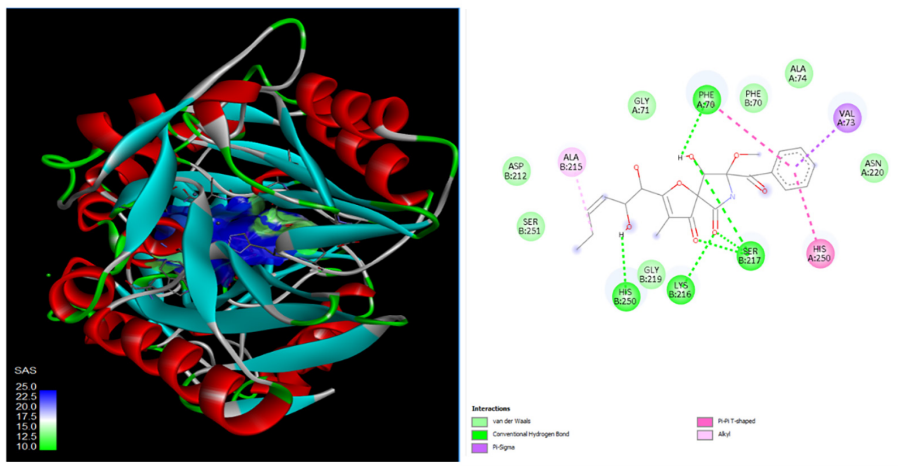 |
| 7VQJ_Scytalone | 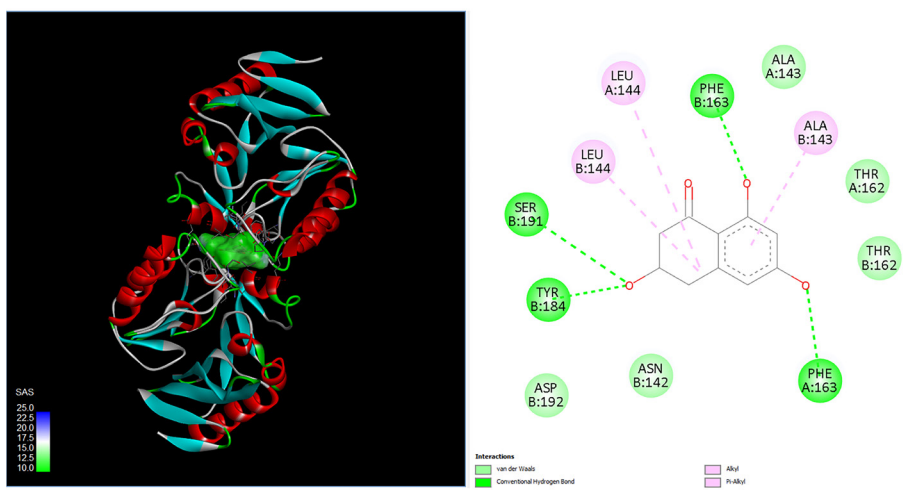 |

***Continued Supplemental Document 1.*** *Discovery Studio Visualizer representation of solvent-accessible surface (SAS) maps and 2D interaction diagrams for selected high-affinity fungal metabolites bound to carbapenemase active sites.*

| | |
|---|---|
| 7VQJ_Pulvinic acid | 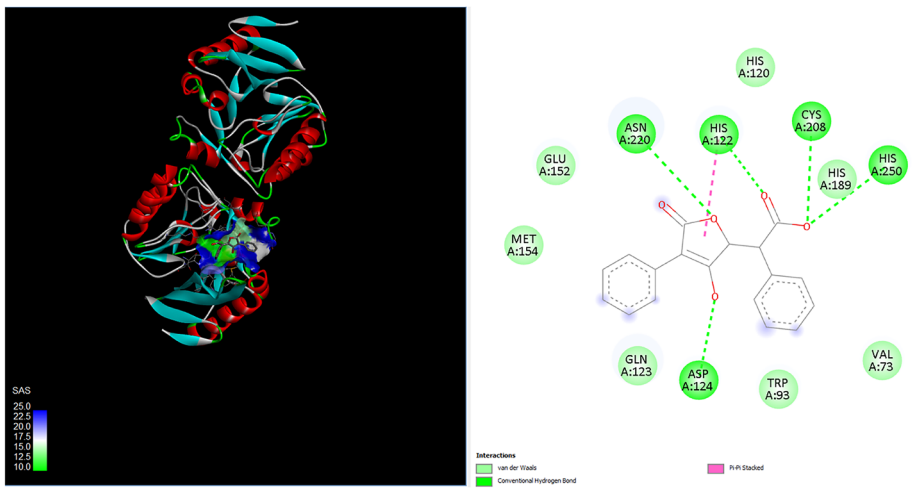 |
| 4EXS_Scytalone | 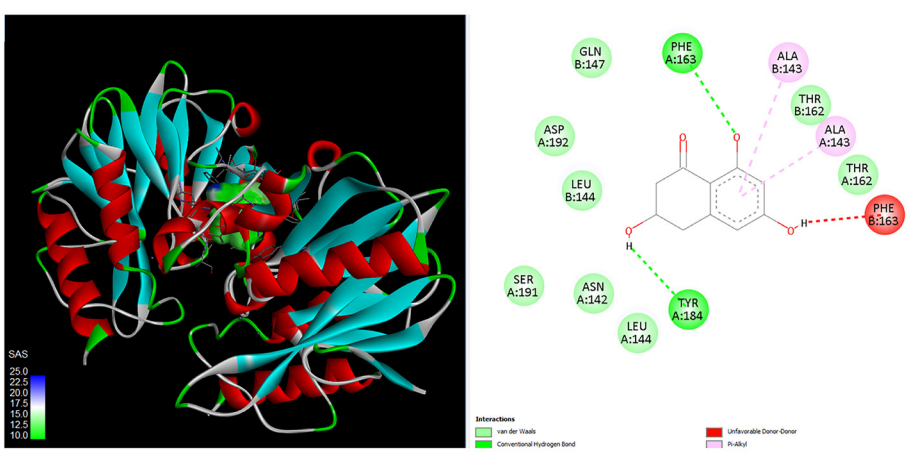 |

***Supplemental Document 2.*** *Computational prediction of ADMET, physicochemical parameters, and drug-likeness characteristics of Hispidin, Pseurotin A, Scytalone, and Pulvinic Acid including BOILED-Egg model, solubility, permeability, metabolic stability, and medicinal chemistry alerts.*

## Hispidin

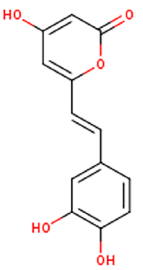


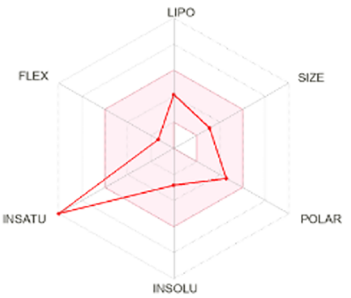


SMILES Oc1cc(/C=C/c2ccc(c(c2)O)O)oc(=O)c1

| Physicochemical Properties | |
|---|---|
| Formula | C13H10O5 |
| Molecular weight | 246.22 g/mol |
| Num. heavy atoms | 18 |
| Num. arom. heavy atoms | 12 |
| Fraction Csp3 | 0.00 |
| Num. rotatable bonds | 2 |
| Num. H-bond acceptors | 5 |
| Num. H-bond donors | 3 |
| Molar Refractivity | 66.42 |
| TPSA | 90.90 Å² |
| **Lipophilicity** | |
| Log $P_{o/w}$ (iLOGP) | 1.61 |
| Log $P_{o/w}$ (XLOGP3) | 1.71 |
| Log $P_{o/w}$ (WLOGP) | 1.71 |
| Log $P_{o/w}$ (MLOGP) | 0.66 |
| Log $P_{o/w}$ (SILICOS-IT) | 2.03 |
| Consensus Log $P_{o/w}$ | 1.54 |

| Water Solubility | |
|---|---|
| Log *S* (ESOL) | -2.81 |
| Solubility | 3.86e-01 mg/ml ; 1.57e-03 mol/l |
| Class | Soluble |
| Log *S* (Ali) | -3.23 |
| Solubility | 1.43e-01 mg/ml ; 5.83e-04 mol/l |
| Class | Soluble |
| Log *S* (SILICOS-IT) | -2.82 |
| Solubility | 3.69e-01 mg/ml ; 1.50e-03 mol/l |
| Class | Soluble |
| **Pharmacokinetics** | |
| GI absorption | High |
| BBB permeant | No |
| P-gp substrate | No |
| CYP1A2 inhibitor | No |
| CYP2C19 inhibitor | No |
| CYP2C9 inhibitor | No |
| CYP2D6 inhibitor | No |
| CYP3A4 inhibitor | No |
| Log $K_p$ (skin permeation) | -6.59 cm/s |
| **Druglikeness** | |
| Lipinski | Yes; 0 violation |
| Ghose | Yes |
| Veber | Yes |
| Egan | Yes |
| Muegge | Yes |
| Bioavailability Score | 0.55 |
| **Medicinal Chemistry** | |
| PAINS | 1 alert: catechol_A |
| Brenk | 1 alert: catechol |
| Leadlikeness | No; 1 violation: MW<250 |
| Synthetic accessibility | 3.04 |

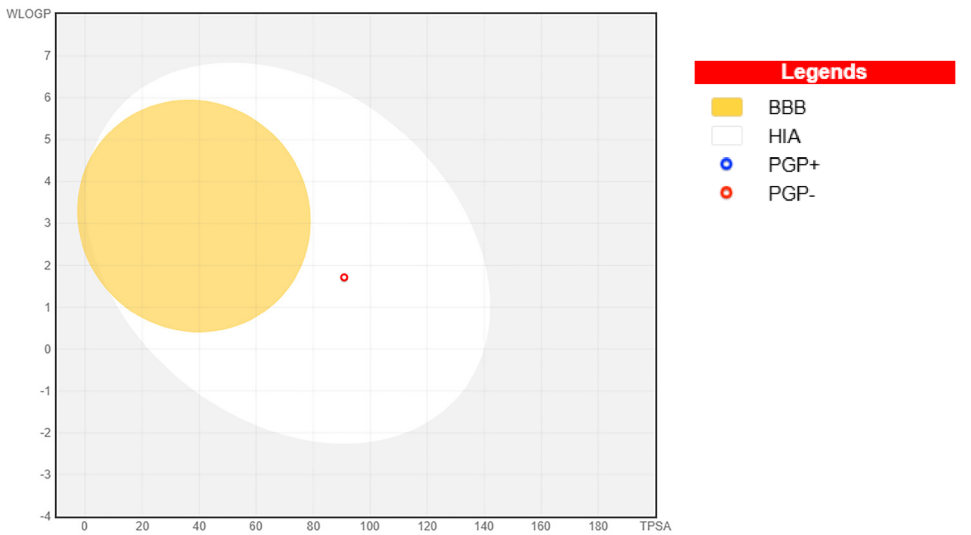

***Continued Supplemental Document 2.*** *Computational prediction of ADMET, physicochemical parameters, and drug-likeness characteristics of Hispidin, Pseurotin A, Scytalone, and Pulvinic Acid including BOILED-Egg model, solubility, permeability, metabolic stability, and medicinal chemistry alerts.*

## Scytalone

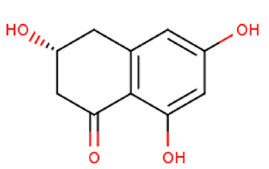


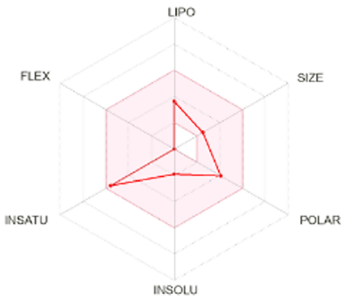


SMILES O[C@H]1CC(=O)c2c(C1)cc(cc2O)O

| Physicochemical Properties | |
|---|---|
| Formula | C10H10O4 |
| Molecular weight | 194.18 g/mol |
| Num. heavy atoms | 14 |
| Num. arom. heavy atoms | 6 |
| Fraction Csp3 | 0.30 |
| Num. rotatable bonds | 0 |
| Num. H-bond acceptors | 4 |
| Num. H-bond donors | 3 |
| Molar Refractivity | 49.50 |
| TPSA | 77.76 Å² |

| Lipophilicity | |
|---|---|
| Log $P_{o/w}$ (iLOGP) | 1.25 |
| Log $P_{o/w}$ (XLOGP3) | 0.89 |
| Log $P_{o/w}$ (WLOGP) | 0.59 |
| Log $P_{o/w}$ (MLOGP) | -0.11 |
| Log $P_{o/w}$ (SILICOS-IT) | 1.09 |
| Consensus Log $P_{o/w}$ | 0.74 |

| Water Solubility | |
|---|---|
| Log *S* (ESOL) | -1.92 |
| Solubility | 2.33e+00 mg/ml ; 1.20e-02 mol/l |
| Class | Very soluble |
| Log *S* (Ali) | -2.11 |
| Solubility | 1.52e+00 mg/ml ; 7.80e-03 mol/l |
| Class | Soluble |
| Log *S* (SILICOS-IT) | -1.44 |
| Solubility | 7.00e+00 mg/ml ; 3.61e-02 mol/l |
| Class | Soluble |

| Pharmacokinetics | |
|---|---|
| GI absorption | High |
| BBB permeant | No |
| P-gp substrate | No |
| CYP1A2 inhibitor | No |
| CYP2C19 inhibitor | No |
| CYP2C9 inhibitor | No |
| CYP2D6 inhibitor | No |
| CYP3A4 inhibitor | No |
| Log $K_p$ (skin permeation) | -6.85 cm/s |

| Druglikeness | |
|---|---|
| Lipinski | Yes; 0 violation |
| Ghose | Yes |
| Veber | Yes |
| Egan | Yes |
| Muegge | No; 1 violation: MW<200 |
| Bioavailability Score | 0.55 |

| Medicinal Chemistry | |
|---|---|
| PAINS | 0 alert |
| Brenk | 0 alert |
| Leadlikeness | No; 1 violation: MW<250 |
| Synthetic accessibility | 2.55 |

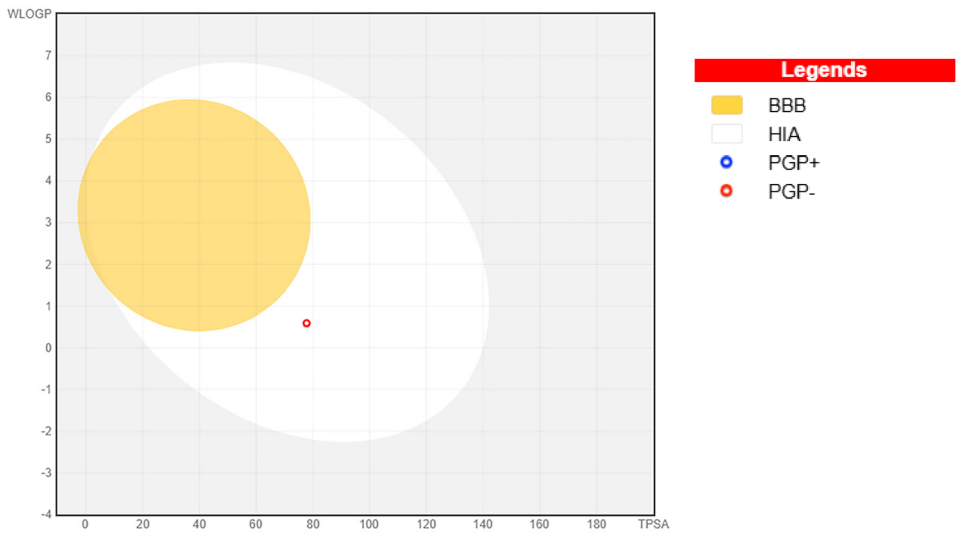

***Supplemental Document 2.*** *Computational prediction of ADMET, physicochemical parameters, and drug-likeness characteristics of Hispidin, Pseurotin A, Scytalone, and Pulvinic Acid including BOILED-Egg model, solubility, permeability, metabolic stability, and medicinal chemistry alerts.*

## Pulvinic Acid

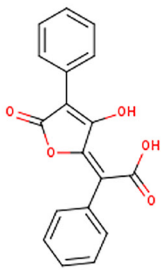


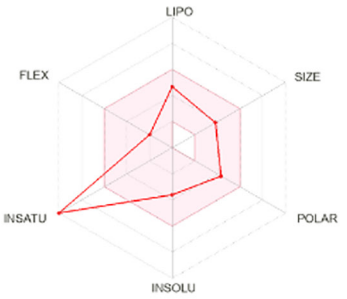


SMILES OC(=O)/C(=C\1/OC(=O)C(=C1O)c1ccccc1)/c1ccccc1

| Physicochemical Properties | |
|---|---|
| Formula | C18H12O5 |
| Molecular weight | 308.28 g/mol |
| Num. heavy atoms | 23 |
| Num. arom. heavy atoms | 12 |
| Fraction Csp3 | 0.00 |
| Num. rotatable bonds | 3 |
| Num. H-bond acceptors | 5 |
| Num. H-bond donors | 2 |
| Molar Refractivity | 83.08 |
| TPSA | 83.83 Å² |

| Lipophilicity | |
|---|---|
| Log $P_{o/w}$ (iLOGP) | 1.99 |
| Log $P_{o/w}$ (XLOGP3) | 2.66 |
| Log $P_{o/w}$ (WLOGP) | 3.01 |
| Log $P_{o/w}$ (MLOGP) | 1.76 |
| Log $P_{o/w}$ (SILICOS-IT) | 2.67 |
| Consensus Log $P_{o/w}$ | 2.42 |

| Water Solubility | |
|---|---|
| Log *S* (ESOL) | -3.62 |
| Solubility | 7.48e-02 mg/ml ; 2.43e-04 mol/l |
| Class | Soluble |
| Log *S* (Ali) | -4.07 |
| Solubility | 2.61e-02 mg/ml ; 8.47e-05 mol/l |
| Class | Moderately soluble |
| Log *S* (SILICOS-IT) | -4.44 |
| Solubility | 1.13e-02 mg/ml ; 3.66e-05 mol/l |
| Class | Moderately soluble |

| Pharmacokinetics | |
|---|---|
| GI absorption | High |
| BBB permeant | No |
| P-gp substrate | No |
| CYP1A2 inhibitor | Yes |
| CYP2C19 inhibitor | No |
| CYP2C9 inhibitor | No |
| CYP2D6 inhibitor | No |
| CYP3A4 inhibitor | No |
| Log $K_p$ (skin permeation) | -6.29 cm/s |

| Druglikeness | |
|---|---|
| Lipinski | Yes; 0 violation |
| Ghose | Yes |
| Veber | Yes |
| Egan | Yes |
| Muegge | Yes |
| Bioavailability Score | 0.56 |

| Medicinal Chemistry | |
|---|---|
| PAINS | 0 alert |
| Brenk | 1 alert: michael_acceptor_1 |
| Leadlikeness | Yes |
| Synthetic accessibility | 3.51 |

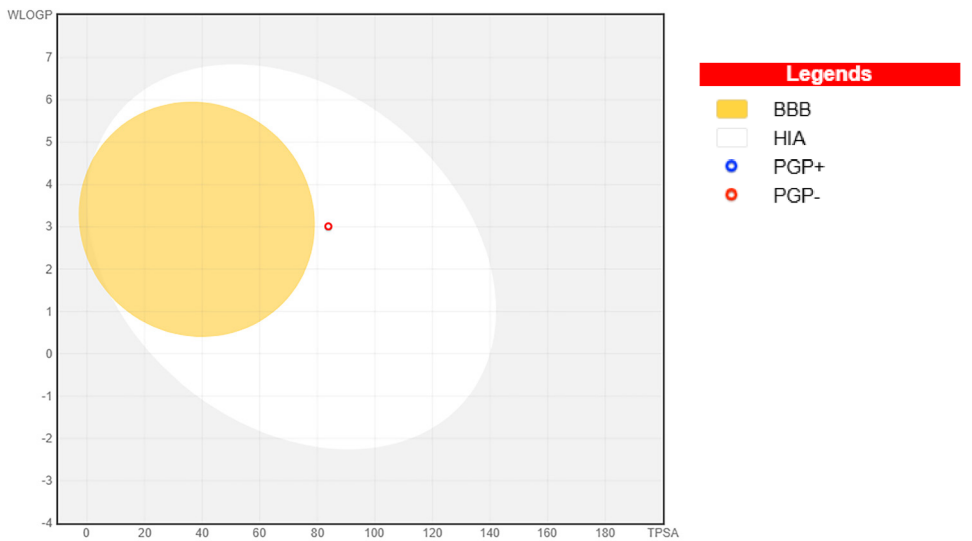

***Continued Supplemental Document 2.*** *Computational prediction of ADMET, physicochemical parameters, and drug-likeness characteristics of Hispidin, Pseurotin A, Scytalone, and Pulvinic Acid including BOILED-Egg model, solubility, permeability, metabolic stability, and medicinal chemistry alerts.*

## Pseurotin A

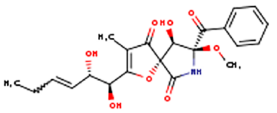

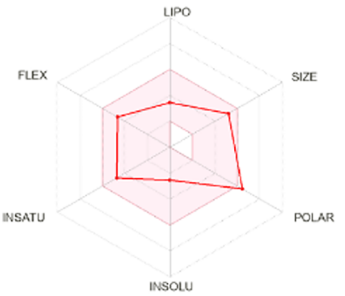


SMILES CC/C=C\[C@@H]([C@@H](C1=C(C)C(=O)[C@]2(O1)C(=O)N[C@@]([C@@H]2O)(OC)C(=O)c1ccccc1)O)O

| Physicochemical Properties | |
|---|---|
| Formula | C22H25NO8 |
| Molecular weight | 431.44 g/mol |
| Num. heavy atoms | 31 |
| Num. arom. heavy atoms | 6 |
| Fraction Csp3 | 0.41 |
| Num. rotatable bonds | 7 |
| Num. H-bond acceptors | 8 |
| Num. H-bond donors | 4 |
| Molar Refractivity | 111.61 |
| TPSA | 142.39 Å² |

| Lipophilicity | |
|---|---|
| Log $P_{o/w}$ (iLOGP) | 2.64 |
| Log $P_{o/w}$ (XLOGP3) | 0.54 |
| Log $P_{o/w}$ (WLOGP) | -0.38 |
| Log $P_{o/w}$ (MLOGP) | -1.58 |
| Log $P_{o/w}$ (SILICOS-IT) | 1.95 |
| Consensus Log $P_{o/w}$ | 0.64 |

| Water Solubility | |
|---|---|
| Log *S* (ESOL) | -2.54 |
| Solubility | 1.25e+00 mg/ml ; 2.91e-03 mol/l |
| Class | Soluble |
| Log *S* (Ali) | -3.10 |
| Solubility | 3.41e-01 mg/ml ; 7.91e-04 mol/l |
| Class | Soluble |
| Log *S* (SILICOS-IT) | -3.23 |
| Solubility | 2.51e-01 mg/ml ; 5.82e-04 mol/l |
| Class | Soluble |

| Pharmacokinetics | |
|---|---|
| GI absorption | Low |
| BBB permeant | No |
| P-gp substrate | Yes |
| CYP1A2 inhibitor | No |
| CYP2C19 inhibitor | No |
| CYP2C9 inhibitor | No |
| CYP2D6 inhibitor | No |
| CYP3A4 inhibitor | No |
| Log $K_p$ (skin permeation) | -8.55 cm/s |

| Druglikeness | |
|---|---|
| Lipinski | Yes; 0 violation |
| Ghose | Yes |
| Veber | No; 1 violation: TPSA>140 |
| Egan | No; 1 violation: TPSA>131.6 |
| Muegge | Yes |
| Bioavailability Score | 0.56 |

| Medicinal Chemistry | |
|---|---|
| PAINS | 0 alert |
| Brenk | 2 alerts: beta_keto_anhydride, isolated_alkene |
| Leadlikeness | No; 1 violation: MW>350 |
| Synthetic accessibility | 5.63 |